Determination of effective conductivities of imperfect contact composites with first-passage simulation

Shih-Yuan Lu* and Chih-Ying Lin
Department of Chemical Engineering, National Tsing-Hua University, Hsin-Chu, Taiwan 30043, Republic of China
(Received 27 June 2003; published 13 November 2003)

A first-passage simulation scheme is developed to determine the effective conductivities of composites with matrix-inclusion interfaces of imperfect contact. The necessary mean hitting probabilities and mean scaled traveling times of the probing walkers in the close vicinity of the imperfect contact interface are derived by solving proposed boundary value problems. The developed scheme is first validated through application in the effective conductivity problem of composites containing periodically arranged spherical inclusions for which accurate results are available for comparison, and is then further applied to the effective conductivity problem of composites containing randomly distributed spherical inclusions. The present development treats the more general imperfect contact problem, with the prefect contact problem as one special case.

DOI: 10.1103/PhysRevE.68.056705 PACS number(s): 02.60.−x, 44.05.+e, 44.10.+i

I. INTRODUCTION

The determination of effective properties for heterogeneous systems has been a classical, important problem in applied physics and engineering. Several different approaches have been developed to treat the problem. These include accurate/approximate solutions of relevant boundary value problems [1–5], construction of upper and lower bounds [6–8], equivalent inclusion models [9,10], and random walk simulations [11,12]. Among them, the random walk simulation is particularly powerful since it can be used for heterogeneous systems of general microstructure and property distribution.

For the steady state heat conduction problem discussed here, the temperature field is governed by the Laplace equation. It is well known that heat conduction can be viewed as a diffusion process of thermal energy, and diffusion processes can be simulated with random walks. Consequently, one can use random walk simulations of sufficiently many probing walkers to study the heat conduction behavior of a material. It can be shown that the mean traveling time needed for a random walker to hit the surface of a d-dimensional sphere of radius R is

$$\tau = R^2/2d\sigma. \tag{1}$$

Here τ is the mean traveling time scaled by the product of material density ρ and specific heat capacity C_p, and σ is the thermal conductivity of the material. Evidently, the higher the conductivity the shorter the mean scaled traveling time needed since the walker can move faster. For composites, there exist at least two different materials of generally different conductivity, and the simulation becomes more complicated. First, the traveling speeds of the walker in materials of different conductivity are different. More importantly, when the walker wanders around in the close vicinity of the interface between two different materials, the walker, at a given walking event, may stay in its starting phase or cross the interface and walk into the other phase, at the expense of some mean scaled traveling time. The relevant mean probability of crossing the interface and the needed mean scaled traveling time for the probing walker have to be properly determined to continue the tracking of the walker [11,12]. Once the mean probability and the mean scaled traveling time for the probing walker wandering at the interface region can be obtained, one can continue the tracking until the walker has probed the composite to a sufficient extent. The effective conductivity of the composite can then be determined as

$$\sigma_{\text{eff}} = X^2/2dT. \tag{2}$$

Here, X is the displacement distance, measured relative to the starting point of the probing walker, and traveled by the probing walker in a mean scaled total traveling time T. To get an accurate probing of the microstructure, one needs to track sufficiently many probing walkers for sufficiently many configurations for a sufficiently long traveling time.

It is, however, rather time consuming to follow the detail zigzag motion of the random walker. A time-saving simulation scheme called the first-passage technique has been developed to replace a great number of zigzag motions of the walker with one single random jump of the walker to the surface of a fictitious d-dimensional sphere lying entirely in a single phase [13,14]. The essential idea is based on Eq. (1). With this, Kim and Torquato [11,12] have successfully developed a first-passage scheme for the computation of effective conductivities for regular and random arrays of aligned long cylinders and spheres under the condition of perfect contact between the matrix and inclusions. It is, however, commonly encountered that the contact between the matrix and inclusions is imperfect [15,16]. There could be contact resistance existing at the matrix-inclusion interface, because of the imperfect contact, giving rise to a discontinuity in temperature field across the interface. This interfacial resistance may be characterized with a dimensionless parameter called the Biot number [1,3]. The matrix-inclusion contact is perfect when the Biot number is infinity while the interface

*Corresponding author. FAX:+886-3-5715408.
Email address: sylu@mx.nthu.edu.tw

becomes perfectly insulating when the Biot number reduces to zero. The perfect contact problem investigated by Kim and Torquato [11,12] is a limiting, special case of the present more general scenario of interfacial resistance problem.

In this paper a first-passage scheme is developed for computation of effective conductivities for regular and random arrays of spheres under the more general situation of interfacial resistance. The necessary mean hitting probability and mean scaled traveling time for probing walkers wandering around in the close vicinity of the interface under the imperfect contact situation are obtained in Sec. II. The resulting first-passage scheme is validated in Sec. III for effective conductivities of the three regular arrays of spheres, namely, simple cubic (sc), body-centered cubic (bcc), and face-centered cubic (fcc), for which accurate results have been obtained by Lu [4] with a boundary collocation scheme and by Cheng and Torquato [5] with the multipole expansion method. The present scheme is then further applied to random arrays of spheres, and comparison with approximate results available from the literature is made. It has to be stressed that the present development can be readily extended to more complicated systems involving nonuniform inclusions with size, conductivity, contact resistance, and even shape distribution, which are difficult, if possible, to tackle with other computational schemes, such as boundary collocation and multipole expansion.

II. THEORY

We consider simulation of the effective conductivity of composites containing regularly or randomly distributed spherical inclusions with a first-passage scheme. The contact between the matrix and inclusions is imperfect such that an interfacial resistance exists at the matrix-inclusion interface, giving rise to a discontinuity in the temperature fields while the normal heat fluxes remain continuous across the interface. This interfacial resistance can be characterized as a convective type resistance and a dimensionless parameter called the Biot number can be defined, as the ratio of the internal conductive resistance to the external convective resistance of the inclusion, to quantify this interfacial resistance. As the external convective resistance diminishes to zero, the Biot number approaches infinity and the situation reduces to the perfect contact case. On the other hand, if the external convective resistance becomes infinitely large, the Biot number goes to zero and the inclusion behaves equivalent to a perfectly insulating inclusion.

To use simulation to determine the effective conductivity of the composite, one throws in sufficiently many probing walkers to the composite and follows the trajectory of each probing walker until the probing walker has explored the composite to a sufficient extent such that a representative average heat conduction behavior of the composite can be derived. An average of the explored results of sufficiently many samplings then gives the effective conductivity of the composite. In the walker tracking process, two pieces of essential information are needed when the probing walker comes to the close vicinity of the interface: the mean probability and the mean scaled traveling time for the probing walker to hit for the first time the surface of a fictitious sphere of radius R centering around the probing walker. Figure 1 shows a probing walker near the interface, which is located at $\mathbf{x}$ and is a distance r away from the interface Γ. The interface divides the fictitious sphere into two regions, one denoted as Ω_1 with a boundary of $\partial\Omega_1$ in the matrix (phase 1) and the other Ω_2 with a boundary of $\partial\Omega_2$ in the inclusion (phase 2). Based on the first-passage theory [17], we propose the following boundary value problems for determination of the relevant mean hitting probability and scaled traveling time functions:

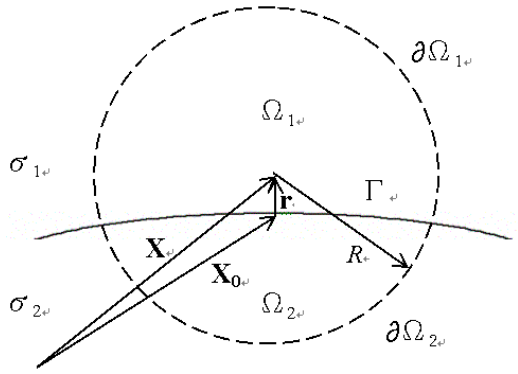

FIG. 1. A schematic for the fictitious sphere around a probing walker that is in the close vicinity of the matrix-inclusion interface.

$$\nabla^2 p_1 = 0 \quad \text{in} \quad \Omega_1 \cup \Omega_2, \tag{3a}$$

$$p_1(\mathbf{x}) = 1 \quad \text{on} \quad \partial\Omega_1, \tag{3b}$$

$$p_1(\mathbf{x}) = 0 \quad \text{on} \quad \partial\Omega_2, \tag{3c}$$

$$\nabla p_1(\mathbf{x}) \cdot \mathbf{n}|_{\Omega_1} = \alpha \nabla p_1(\mathbf{x}) \cdot \mathbf{n}|_{\Omega_2} = (B_i/a)[p_1(\mathbf{x})|_{\Omega_1} - p_1(\mathbf{x})|_{\Omega_2}] \quad \text{on} \quad \Gamma, \tag{3d}$$

and

$$\sigma_i \nabla^2 \tau_s = -1 \quad \text{in} \quad \Omega_i, \tag{4a}$$

$$\tau_s(\mathbf{x}) = 0 \quad \text{on} \quad \partial\Omega_1 \cup \partial\Omega_2, \tag{4b}$$

$$\nabla \tau_s(\mathbf{x}) \cdot \mathbf{n}|_{\Omega_1} = \alpha \nabla \tau_s(\mathbf{x}) \cdot \mathbf{n}|_{\Omega_2} = (B_i/a)[\tau_s(\mathbf{x})|_{\Omega_1} - \tau_s(\mathbf{x})|_{\Omega_2}] \quad \text{on} \quad \Gamma. \tag{4c}$$

Here p_1 is the probability of the probing walker hitting $\partial\Omega_1$ for the first time without hitting $\partial\Omega_2$, τ_s is the mean traveling time, scaled by the product of relevant phase density and specific heat capacity, for the probing walker to hit $\partial\Omega_1 \cup \partial\Omega_2$ for the first time, σ_1 and σ_2 are the conductivities of the matrix and inclusion, respectively, α is the conductivity ratio of σ_2 to σ_1, $\mathbf{n}$ is the outward unit vector normal to Γ, a is the radius of the inclusion, B_i defined as ha/σ_2 is the Biot number, and the reciprocal of h is the

convective resistance at the interface. Note that $p_2(\mathbf{x})=1-p_1(\mathbf{x})$ by definition. The discontinuities in the $p_1(\mathbf{x})$ and $\tau_s(\mathbf{x})$ fields across the interface are imposed to take into account the interfacial resistance, while their normal fluxes remain continuous. Additionally, the boundary conditions (3b), (3c), and (4b) arise naturally from the definitions of p_1 and τ_s.

The above two boundary value problems can be solved numerically to find $p_1(\mathbf{x})$ and $\tau_s(\mathbf{x})$ with the boundary collocation method. The basic idea of the boundary collocation method is to first construct a suitable basis solution, which carries some unknown coefficients and satisfies the governing equation identically but not necessarily the boundary conditions, and then to force the basis solution to satisfy boundary conditions at properly chosen points located on the relevant boundaries to solve for the unknown coefficients. The end result is a linear equation set solving which determines the unknown coefficients and thus the complete basis solution.

For $p_1(\mathbf{x})$, a linear combination of the spherical harmonic functions is a natural choice:

$$p_1(\mathbf{x})|_{\Omega_1}=a_0^I+\sum_{n=1}^{\infty} a_n^I\left(\frac{r}{R}\right)^n P_n(\mu), \tag{5a}$$

$$p_1(\mathbf{x})|_{\Omega_2}=a_0^{II}+\sum_{n=1}^{\infty} a_n^{II}\left(\frac{r}{R}\right)^n P_n(\mu). \tag{5b}$$

Here, a_0^I, a_0^{II}, a_n^I, and a_n^{II} are unknown coefficients to be determined with the boundary collocation procedure, P_n the nth order Legendre function of the first kind, μ a short notation for $\cos\theta$, and (r,θ,ϕ) the spherical coordinates. The problem is axisymmetric and thus there is no ϕ dependence. Also harmonic functions involving r^{-n} are not included since p_1 should remain finite as r tends to zero. The unknown coefficients can be readily determined with imposition of Eqs. (3b) to (3d) at chosen points located on Γ, $\partial\Omega_1$, and $\partial\Omega_2$.

As for τ_s, an extra term accounting for the particular solution of the Poisson equation should be included,

$$\left.\frac{\tau_s(\mathbf{x})}{R^2/6\sigma_1}\right|_{\Omega_1}=b_0^I+\sum_{n=1}^{\infty} b_n^I\left(\frac{r}{R}\right)^n P_n(\mu)-\left(\frac{r}{R}\right)^2, \tag{6a}$$

$$\left.\frac{\tau_s(\mathbf{x})}{R^2/6\sigma_1}\right|_{\Omega_2}=b_0^{II}+\sum_{n=1}^{\infty} b_n^{II}\left(\frac{r}{R}\right)^n P_n(\mu)-\frac{1}{\alpha}\left(\frac{r}{R}\right)^2. \tag{6b}$$

Here, again b_0^I, b_0^{II}, b_n^I, and b_n^{II} are unknown coefficients to be determined with the boundary collocation procedure. The mean scaled traveling time is normalized with the mean scaled traveling time of the probing walker wandering in the matrix for a distance R. Note that one needs to truncate the summations involved in Eqs. (5a), (5b), (6a), and (6b) at a finite term, say N, to allow for numerical computation. A setting of 30 for N gives satisfactory results.

An approximate analytical solution can be derived if one restricts the size of the fictitious sphere to be relatively small as compared to the inclusion size such that the local interface Γ can be taken approximately as a flat plane dividing the sphere into two equal halves. In the following, we present the analytical solutions for p_1 and τ_s in domains Ω_1 and Ω_2 for the flat interface approximation:

$$p_1(r,\theta)=\frac{H(r)+B_i^*}{B_i^*(\alpha+1)+H(r)}+\frac{B_i^*\alpha}{B_i^*\alpha+H(r)+B_i^*}\sum_{m=0}^{\infty} b_m\left(\frac{r}{R}\right)^{2m+1}P_{2m+1}(\mu)$$

$$\text{for } 0\leqslant r\leqslant R,\quad 0\leqslant\theta\leqslant\pi/2, \tag{7a}$$

$$p_1(r,\theta)=\frac{B_i^*}{B_i^*(\alpha+1)+H(r)}\times\left[1+\sum_{m=0}^{\infty} b_m\left(\frac{r}{R}\right)^{2m+1}P_{2m+1}(\mu)\right]$$

$$\text{for } 0\leqslant r\leqslant R,\quad \pi/2\leqslant\theta\leqslant\pi, \tag{7b}$$

$$H(r)=\sum_{m=0}^{\infty}\frac{[(2m)!]^2(4m+3)(2m+1)}{2^{4m+1}(m!)^4(m+1)}\left(\frac{r}{R}\right)^{2m}, \tag{7c}$$

$$b_m=\frac{(-1)^m(2m)!(4m+3)}{2^{2m+1}(m!)^2(m+1)}, \tag{7d}$$

$$\frac{\tau_s(r,\theta)}{R^2/6\sigma_1}=(1+c^I)+3c^I\sum_{m=0}^{\infty} c_m\left(\frac{r}{R}\right)^{2m+1}P_{2m+1}(\mu)+\left(\frac{r}{R}\right)^2[2c^IP_2(\mu)-1]$$

$$\text{for } 0\leqslant r\leqslant R,\quad 0\leqslant\theta\leqslant\pi/2, \tag{8a}$$

$$\frac{\tau_s(r,\theta)}{R^2/6\sigma_1}=\frac{1}{\alpha}\left\{1-c^I+3c^I\sum_{m=0}^{\infty} c_m\left(\frac{r}{R}\right)^{2m+1}P_{2m+1}(\mu)-\left(\frac{r}{R}\right)^2[2c^IP_2(\mu)+1]\right\}$$

$$\text{for } 0\leqslant r\leqslant R,\quad \pi/2\leqslant\theta\leqslant\pi, \tag{8b}$$

$$c^I=\frac{B_i^*(\alpha-1)\left[1-\left(\frac{r}{R}\right)^2\right]}{3K(r)-B_i^*(1+\alpha)\left[1-\left(\frac{r}{R}\right)^2\right]}, \tag{8c}$$

$$c_m=\frac{4m+3}{(m+1)(m+2)(2m-1)}\frac{(-1)^m(2m)!}{2^{2m+1}(m!)^2}, \tag{8d}$$

$$K(r)=\sum_{m=0}^{\infty}\left[\frac{(-1)^m(2m)!}{2^{2m+1}(m!)^2}\frac{4m+3}{m+1}\right]\times\left[\frac{(-1)^m(2m)!}{2^{2m}(m!)^2}\right]\frac{2m+1}{(m+2)(2m-1)}\left(\frac{r}{R}\right)^{2m}. \quad (8e)$$

Here, B_i^* equals $B_i(R/a)$. The above results reduce correctly to the corresponding equations derived by Kim and Torquato [11] for the special case of perfect contact as B_i tends to infinity. In Sec. III results for p_1 and τ_s coming from the above derivations are found to agree well with those from the accurate boundary collocation calculation.

For simulation purposes, one needs only p_1 and τ_s values at θ of 0 and π since one can always situate the probing walker on the symmetric axis normal to the interface. When the probing walker is in a single phase, it moves according to the first-passage concept. One first constructs the largest possible fictitious sphere that does not intercept with any part of the other phase, and then sets a random moving direction through suitable random numbers. With this moving procedure, the probing walker would very rarely, if not never, exactly hit the interface. One thus needs to define a thin layer within which the probing walker is claimed to be close enough to the interface and is possible to cross the interface, spending a mean scaled traveling time τ_s, according to the mean hitting probability p_1. Also, one needs a jumping distance R when moving within the interfacial thin layer. Let us define δ_1 to be the ratio of the thin layer thickness to a and δ_2 to be the ratio of the interfacial jumping distance to a. The magnitude of δ_1 should be kept small enough to avoid excessive simulation errors, but not too small to lengthen the simulation time. As for δ_2, it has to be relatively large as compared to δ_1 to save simulation time and to suppress errors induced by a nonzero δ_1. In the present study, the settings of 0.003 for δ_1 and 0.03 for δ_2 give satisfactory results.

Since practically the ratio of δ_1 to δ_2 is only a small number, say 0.01 for our setting here, one needs to pay attention to p_1 and τ_s at locations with a small r/R, say less than 0.01. In the following, we present the flat interface approximation expressions for p_1 and τ_s at $r/R=0$ and $\theta=0$ and π. These expressions should give us a quick understanding of the characteristics of p_1 and τ_s, particularly at the two limiting scenarios of perfect contact and perfect insulation,

$$p_1(r=0,0)=\frac{3+2B_i^*}{2B_i^*(\alpha+1)+3}\rightarrow\begin{cases}1 & \text{as } B_i^*\rightarrow 0\\ 1/(1+\alpha) & \text{as } B_i^*\rightarrow\infty,\end{cases} \quad (9a)$$

$$p_1(r=0,\pi)=\frac{2B_i^*}{2B_i^*(\alpha+1)+3}\rightarrow\begin{cases}0 & \text{as } B_i^*\rightarrow 0\\ 1/(1+\alpha) & \text{as } B_i^*\rightarrow\infty,\end{cases} \quad (9b)$$

$$\tau_s(r=0,0)/\tau_1=\frac{9+8B_i^*}{9+4(1+\alpha)B_i^*}\rightarrow\begin{cases}1 & \text{as } B_i^*\rightarrow 0\\ 2/(1+\alpha) & \text{as } B_i^*\rightarrow\infty,\end{cases} \quad (9c)$$

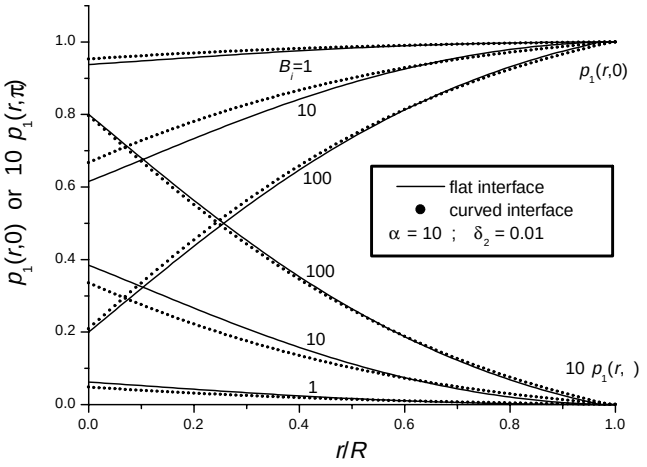

FIG. 2. Plot of p_1 vs r/R for the case of $\alpha=10$ and $\delta_2=0.01$ for three B_i $(=1,10,100)$.

$$\tau_s(r=0,\pi)/\tau_1=\frac{1}{\alpha}\frac{9+8\alpha B_i^*}{9+4(1+\alpha)B_i^*}\rightarrow\begin{cases}1/\alpha & \text{as } B_i^*\rightarrow 0\\ 2/(1+\alpha) & \text{as } B_i^*\rightarrow\infty.\end{cases} \quad (9d)$$

Here, τ_1 is $R^2/6\sigma_1$ representing the mean scaled traveling time if the probing walker is let wander in phase 1 for a distance R. Evidently, the probing walker can only stay in its starting phase $[p_1(r=0,0)=1$ and $p_1(r=0,\pi)=0]$ when the interface is in perfect insulation $(B_i^*\rightarrow 0)$, and the probing walker will spend a mean scaled traveling time of τ_1 as it were traveling in a single phase $[\tau_s(r=0,0)/\tau_1=1$ and $\tau_s(r=0,\pi)/\tau_1=1/\alpha]$. While for the perfect contact situation $(B_i^*\rightarrow\infty)$, the probing walker hits the surface of the fictitious sphere located in phase 1 according to the relative easiness of traveling in phase 1 $[p_1(r=0,0)=p_1(r=0,\pi)=1/(1+\alpha)]$, and spends a weighted average mean scaled traveling time $[\tau_s(r=0,0)/\tau_1=\tau_s(r=0,0\pi)/\tau_1=2/(1+\alpha)]$. Here, the weighted average mean scaled traveling time can be derived as the following:

$$\tau_1\times p_1(r=0,0)+\tau_2\times p_1(r=0,\pi)=\frac{\tau_1}{1+\alpha}+\frac{\tau_1}{\alpha}\frac{\alpha}{1+\alpha}=\frac{2\tau_1}{1+\alpha}. \quad (10)$$

Here τ_2 is equal to $R^2/6\sigma_2$ representing the mean scaled traveling time if the probing walker is let wander in phase 2 for a distance R.

III. RESULTS AND DISCUSSION

A. Characteristics of p_1 and τ_s

We first study the characteristics of p_1 and τ_s. Figure 2 shows $p_1(r,0)$ and $p_1(r,\pi)$ vs r/R with Bi as the varying

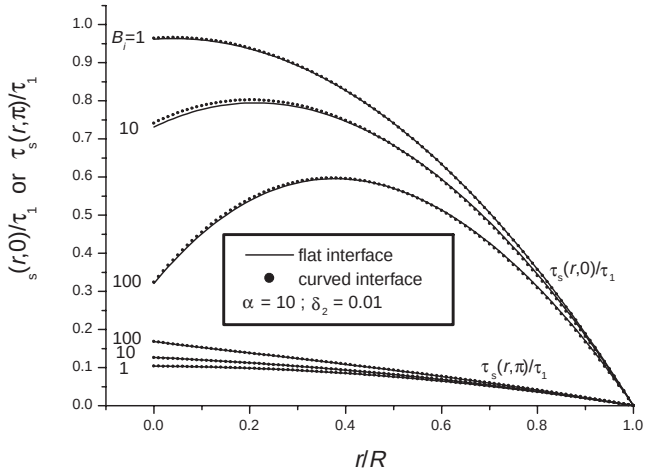

FIG. 3. Plot of τ_s vs r/R for the case of $\alpha=10$ and $\delta_2=0.01$ for three B_i $(=1,10,100)$.

parameter. Both results for flat interface approximation and accurate boundary collocation calculation are presented for the case of $\alpha=10$ and $\delta_2=0.01$. There are several points to note. First, the two calculations agree with each other quite well, with the largest discrepancy occurring at the intermediate B_i. The discrepancy comes from the flat interface approximation. In fact, the true interface concaves towards the inclusion, and one expects the flat interface approximation to underestimate $p_1(r,0)$ and overestimate $p_1(r,\pi)$.

The discontinuity in p_1 at the interface $(r/R=0)$ is clearly shown in the plot. This discontinuity is a direct result of the interfacial resistance, and shrinks as B_i increases towards the perfect contact limit. When B_i decreases, the interfacial resistance increases and the possibility for the probing walker originally located in phase 2 to cross the interface and jump onto the surface of the fictitious sphere in phase 1, $p_1(r,\pi)$, decreases. On the contrary, it becomes more likely for the probing walker originally located in phase 1 to hit the surface of the fictitious sphere in phase 1, $p_1(r,0)$, since it is now more difficult for the probing walker to cross the interface. With further decrease in B_i, $p_1(r,0)$ will approach unity, while $p_1(r,\pi)$ tends to zero, as indicated by Eqs. (9a) and (9b).

As for the study of the mean scaled traveling time τ_s, we plot in Fig. 3 $\tau_s(r,0)/\tau_1$ and $\tau_s(r,\pi)/\tau_1$ vs r/R with B_i as the varying parameter for the case of $\alpha=10$ and $\delta_2=0.01$. Again, the flat interface approximation agrees well with the accurate boundary collocation calculation. The underestimation for $\tau_s(r,0)/\tau_1$ and overestimation for $\tau_s(r,\pi)/\tau_1$ of the flat interface approximation result from the deviation of the true interface shape from a flat plane. Since the true interface concaves towards the more conducting inclusion (phase 2), there is in fact a larger portion of the volume of the fictitious sphere occupied by the less conducting phase 1, in which probing walkers travel slower and need a longer mean scaled traveling time to reach the sphere surface. With the same logic, one can explain why there is an overestimation for $\tau_s(r,\pi)/\tau_1$ given by the flat interface approximation.

The discontinuity in τ_s at the interface is evident from the figure. As B_i increases, the discontinuity shrinks as expected. While with decreasing B_i, $\tau_s(r=0,0)/\tau_1$ tends to unity and $\tau_s(r=0,\pi)/\tau_1$ approaches τ_2/τ_1 $(=1/\alpha)$ since the interface becomes more difficult to cross and probing walkers tend to stay in their original phases traveling as though they were in a single phase environment. Also note that the curves for $\tau_s(r,0)/\tau_1$ exhibit maxima. This can be explained as follows. When the starting location of the probing walker moves away from the interface, the probing walker will have less chance to travel in the more conducting and thus more speedy phase 2, and as a result the mean scaled traveling time increases. But when the probing walker moves closer to its destiny, the surface of the fictitious sphere, the distance it has to travel reduces, and the mean scaled traveling time decreases. The end result is a maximum in $\tau_s(r,0)/\tau_1$. As B_i decreases, the location of this maximum $\tau_s(r,0)/\tau_1$ moves towards the interface since the interface becomes more difficult to cross and thus the influence of the possible travel in phase 2 lessens.

Although the flat interface approximation approaches the accurate boundary collocation calculation quite well, it is found not to be good enough to replace the accurate boundary collocation calculation in the first passage simulation. In fact, the discrepancy in p_1 and τ_s between results from the two methods is found to depend not only on α and δ_2 but also on B_i. It is too difficult to construct a correction factor as a function of the three parameters; therefore, we use the accurate boundary collocation calculation for all first-passage simulations performed in this work. The flat interface approximation, however, helps to capture the physical insight of the scheme.

B. Validation by comparison with results from periodic composites

To validate the present development, we compute effective conductivities for periodic composites (sc, bcc, and fcc) of finite B_i^* containing regularly arranged spheres. For these types of periodic composites of finite B_i^*, Lu [4] and Cheng and Torquato [5] computed the accurate effective conductivity with a boundary collocation scheme and a multipole expansion method, respectively. Here, in Figs. 4–6 we show the comparison results for sc, bcc, and fcc arrays of $\alpha=10$ and $B_i=0.2$ and 1/30, respectively. The present development agrees quite well with the accurate calculation. Note that for composites with interfacial resistances, there exists a critical B_i $[=1/(\alpha-1)]$ at which the effective conductivity of the composite is exactly unity [2–4], meaning that the enhancing effect of the inclusion is exactly balanced by the impairing effect of the interfacial resistance. The effective conductivity increases with an increasing volume fraction of the inclusion if B_i is set above the critical B_i. On the other hand, the effective conductivity decreases with an increasing volume fraction of the inclusion if B_i is set below the critical B_i. For the case of $\alpha=10$, the critical B_i is 1/9, and this is why the curves of $B_i=0.2$ go up while the curves of $B_i=1/30$ go down in the figures with increasing f. The simulation results

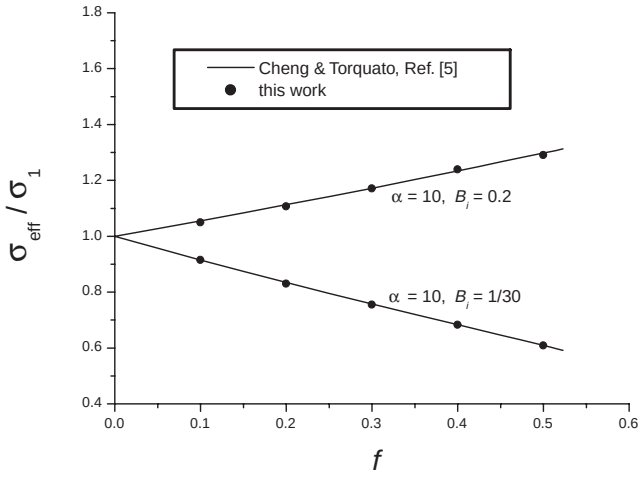

FIG. 4. Normalized effective conductivity vs the inclusion volume fraction for simple-cubic spherical arrays for the case of $\alpha=10$ and $B_i=0.2$ and 1/30 as obtained from the present simulation and from the accurate calculation of Cheng and Torquato [5].

are averages of 100 runs with each run obtained from following 200 probing walkers for a total displacement of 100 to 300 $(X/a)^2$.

C. Results for random arrays

We further apply the present development to random spherical arrays. The random arrays are generated with the Metropolis algorithm [18]. The essence of the algorithm is to first arrange inclusions in a regular array in a unit cell, and then to randomize the array by moving each inclusion in a random direction, under the restriction of nonoverlapping, sufficiently many times. The usual periodic boundary condition is imposed to extend the unit cell to represent an infinitely large composite space. Here, we use both the body-centered-cubic and face-centered-cubic arrays as the starting regular arrays to generate the random spherical arrays, and

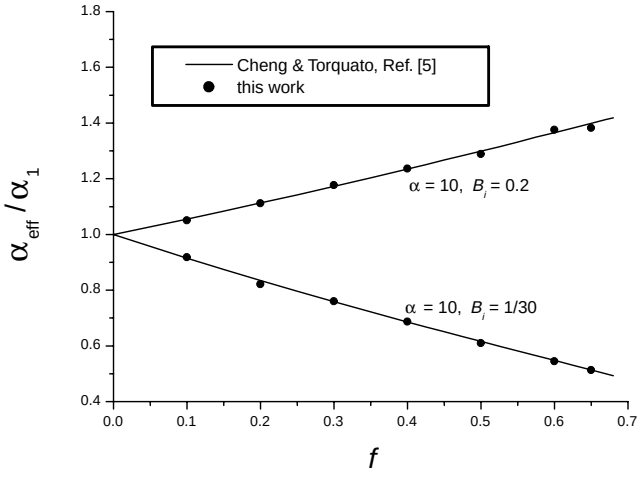

FIG. 5. Normalized effective conductivity vs the inclusion volume fraction for body-centered-cubic spherical arrays for the case of $\alpha=10$ and $B_i=0.2$ and 1/30 as obtained from the present simulation and from the accurate calculation of Cheng and Torquato [5].

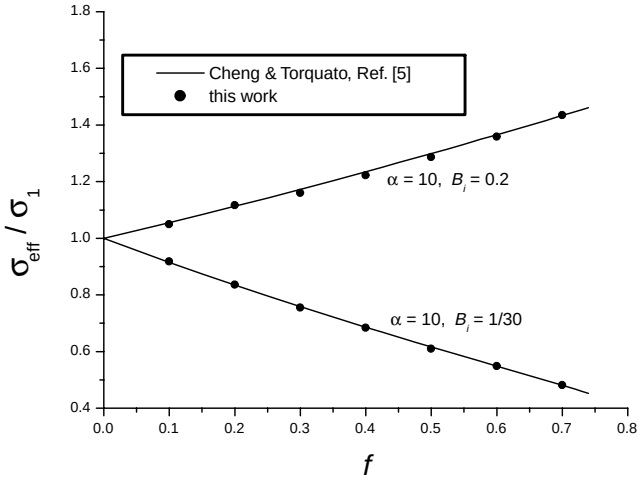

FIG. 6. Normalized effective conductivity vs the inclusion volume fraction for face-centered-cubic spherical arrays for the case of $\alpha=10$ and $B_i=0.2$ and 1/30 as obtained from the present simulation and from the accurate calculation of Cheng and Torquato [5].

we move each inclusion at least 1000 times. The number of particles used in a unit cell has to be large enough to ensure sufficient randomness of the array. We generate the random arrays with 16, 32, and 54 spheres per unit cell (N_p) to test the convergence of the effective conductivity result with respect to the particle number used. Again, the simulation results are obtained from the average of 100 realizations with each realization probed by 200 random walkers for a total displacement of 100 to 300 $(X/a)^2$.

Chiew and Glandt [1] have investigated the same problem by taking into account rigorous thermal interactions between particles up to the pair interaction level such that their results are accurate to the $O(f^2)$ terms,

$$\frac{\sigma_{\rm eff}}{\sigma_1}=\frac{1+2\theta_1 f+(K_2-3\theta_1^2)f^2}{1-\theta_1 f}, \tag{11a}$$

with

$$\theta_1=\frac{B_i(\sigma_2-1)-1}{B_i(\sigma_2+2)+2}. \tag{11b}$$

Here K_2 is a function of the pair correlation function of equilibrium hard-sphere fluids and the dimensionless multipole polarizability of the thermal interactions. Here, θ_1 is the relevant dimensionless dipole polarizability. Interested readers can consult Chiew and Glandt [1] for details. In addition, it was mentioned in Cheng and Torquato [5] that Torquato and Rintoul derived a good approximate formula for the present problem:

$$\frac{\sigma_{\rm eff}}{\sigma_1}=\frac{1+2f\theta_1-2(1-f)\varsigma_2\theta_1^2}{1-f\theta_1-2(1-f)\varsigma_2\theta_1^2}, \tag{12}$$

where ς_2 is a three-point microstructural parameter that has been tabulated for random spherical arrays by Miller and Torquato [8].

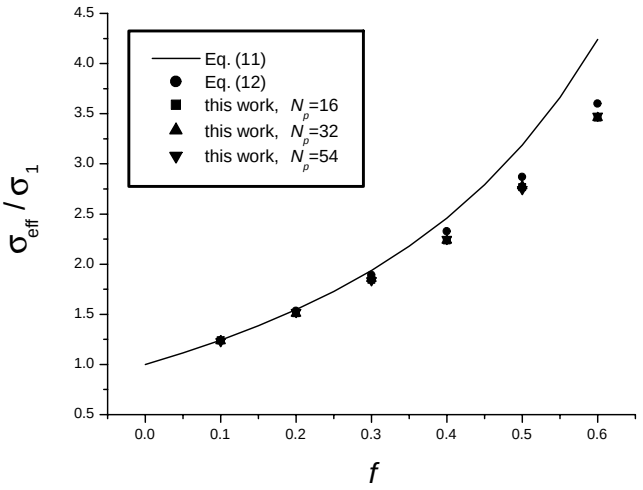

FIG. 7. Normalized effective conductivity vs the inclusion volume fraction for random spherical arrays for the case of $\alpha=10$ and $B_i=10$ as obtained from the present simulation and the two approximate formulas, Eqs. (11) and (12).

Figure 7 shows the effective conductivity results obtained with the present development and the aforementioned two approximations for the random spherical arrays for the case of $\alpha=10$ and $B_i=10$. There are several points to note. First, the convergence test with respect to the particle number is satisfactory as can be seen from the overlap of the three sets of data for N_p of 16, 32, and 54. Second, the pair interaction approach overestimates the effective conductivity at higher inclusion volume fractions, which is not surprising since at higher f particle interactions beyond the pair interaction level are needed. Third, the approximate formula given in Eq. (12) gives good estimates even at high f. Its success may be due to the accurate account of the system microstructure.

IV. CONCLUSION

We have developed a first-passage simulation scheme for the computation of effective conductivities of composites with interfacial resistance at the matrix-inclusion interface. The scheme is illustrated with the computation of effective conductivities of two-phase composites containing regularly or randomly distributed spheres. It is, however, worth mentioning that the scheme can be readily extended to multiphase composites in which inclusions of different conductivity are present. Since the interfacial region concerned in the simulation process is a local, small region and is irrelevant to the shape of the inclusion, the scheme is also expected to be applicable to composites containing inclusions with shape other than spherical provided that the inclusion shape is smooth enough without sharp corners or sharp angles. Furthermore, composites containing inclusions of a size distribution can also be treated with the present scheme.

ACKNOWLEDGMENTS

The authors gratefully acknowledge the support of the National Science Council of the Republic of China under Grant No. NSC 89-2214-E-007-028. Part of the calculation of this work was carried out on the computing resources offered by the National Center for High-Performance Computing of the Republic of China.

[1] Y. C. Chiew and E. D. Glandt, Chem. Eng. Sci. **42**, 2677 (1987).
[2] S.-Y. Lu and H.-C. Lin, Chem. Eng. Sci. **50**, 2611 (1995).
[3] S.-Y. Lu and J.-L. Song, Chem. Eng. Sci. **51**, 4393 (1996).
[4] S.-Y. Lu, J. Colloid Interface Sci. **192**, 386 (1997).
[5] H. Cheng and S. Torquato, Proc. R. Soc. London **A453**, 145 (1997).
[6] G. W. Milton, J. Appl. Phys. **52**, 5294 (1981).
[7] S. Torquato and F. Lado, Phys. Rev. B **33**, 6428 (1986).
[8] C. A. Miller and S. Torquato, J. Appl. Phys. **68**, 5486 (1990).
[9] S.-Y. Lu, J. Chin. Inst. Chem. Eng. **29**, 139 (1998).
[10] S.-Y. Lu, J. Appl. Phys. **84**, 2647 (1998).
[11] I. C. Kim and S. Torquato, J. Appl. Phys. **68**, 3892 (1990).
[12] I. C. Kim and S. Torquato, J. Appl. Phys. **69**, 2280 (1991).
[13] S. Torquato and I. C. Kim, Appl. Phys. Lett. **55**, 1847 (1989).
[14] L. Zheng and Y. C. Chiew, J. Chem. Phys. **90**, 322 (1989).
[15] D. P. H. Hasselman, K. Y. Donaldson, and A. L. Geiger, J. Am. Ceram. Soc. **75**, 3137 (1992).
[16] R. Ruh, K. Y. Donaldson, and D. P. H. Hasselman, J. Am. Ceram. Soc. **75**, 2887 (1992).
[17] S. Lifson and J. L. Jackson, J. Chem. Phys. **36**, 2410 (1962).
[18] N. Metropolis, A. W. Rosenbluth, M. N. Rosenbluth, A. N. Teller, and E. Teller, J. Chem. Phys. **21**, 1087 (1953).